Asian Journal of Pharmaceutical Sciences 18 (2023) 100832

Available online at www.sciencedirect.com

ScienceDirect

journal homepage: www.elsevier.com/locate/AJPS

Original Research Paper

pH-triggered dynamic erosive small molecule chlorambucil nano-prodrugs mediate robust oral chemotherapy ☆

Xin Liu[1], *Zhexiang Wang*[1], *Xiaodie Ren*, *Xinyang Chen*, *Jinjin Tao*, *Yuanhui Guan*, *Xuefeng Yang*, *Rupei Tang**, *Guoqing Yan**

Engineering Research Center for Biomedical Materials, Anhui Key Laboratory of Modern Biomanufacturing, School of Life Sciences, Anhui University, Hefei 230601, China

ARTICLE INFO

Article history:
Received 8 March 2023
Revised 5 May 2023
Accepted 30 June 2023
Available online 25 July 2023

Keywords:
Nano-prodrugs
pH sensitivity
Size transition
Oral chemotherapy

ABSTRACT

Currently, the dynamic erosive small molecule nano-prodrug is of great demand for oral chemotherapy, owing to its precise structure, high drug loading and improved oral bioavailability via overcoming various physiologic barriers in gastrointestinal tract, blood circulation and tumor tissues compared to other oral nanomedicines. Herein, this work highlights the successful development of pH-triggered dynamic erosive small molecule nano-prodrugs based on *in vivo* significant pH changes, which are synthesized via amide reaction between chlorambucil and star-shaped ortho esters. The precise nano-prodrugs exhibit extraordinarily high drug loading (68.16%), electric neutrality, strong hydrophobicity, and dynamic large-to-small size transition from gastrointestinal pH to tumoral pH. These favorable physicochemical properties can effectively facilitate gastrointestinal absorption, blood circulation stability, tumor accumulation, cellular uptake, and cytotoxicity, therefore achieving high oral relative bioavailability (358.72%) and significant tumor growth inhibition while decreasing side effects. Thus, this work may open a new avenue for robust oral chemotherapy attractive for clinical translation.

1. Introduction

Oral chemotherapy as an appealing treatment for cancer has been always considered the most convenient way to deliver the chemotherapeutics [1]. Unfortunately, multiple physiologic barriers associated to oral administration in gastrointestinal tract (GIT), liver, blood vessel and tumor tissue lead to high clearance, low bioavailability, serious side effects and unsatisfactory treatment [2,3]. Oral nanomedicines have attracted much attention in recent years, because they not only can increase drug solubility, but also can improve drug

☆ Peer review under responsibility of Shenyang Pharmaceutical University.

* Corresponding authors.
E-mail addresses: tangrp99@iccas.ac.cn (R. Tang), 17017@ahu.edu.cn (G. Yan).
[1] These authors contribute equally.
Peer review under responsibility of Shenyang Pharmaceutical University.

https://doi.org/10.1016/j.ajps.2023.100832

bioavailability via protecting chemotherapeutic drugs from unfavorable biological and physicochemical conditions in the GIT, and avoiding first-pass metabolism in liver [4–6]. However, most of them exhibit poor tumor selectivity after suffering from *in vivo* multiple barriers, and exist as drug-embedded nanoparticles (NPs), which show imprecise regulation over drug constituent, carrier structure as well as each batch drug loading and release [7]. These disadvantages hinder further clinical transformation and force us to develop a programable oral nanomedicine with defined structure, high drug loading, and enhanced drug bioavailability for robust oral chemotherapy while significantly decreasing side effects.

Stimuli-responsive small molecule nano-prodrugs that not only maintain nanoscale advantages, but also endow the characteristics of convenient synthesis, precise structure, extraordinary drug loading capacity and programmable targeted drug release, have tremendous potential for ideal oral chemotherapy [8,9]. Moreover, significant pH changes exist among stomach (pH 1.0–3.0), small intestine (duodenum pH 4.0–5.5, jejunum pH 5.5–7.0 and ileum pH 7.0–7.5), blood vessel (pH 7.4) and tumor tissue (extracellular matrix pH 6.5–7.0, endosome pH 5.0–6.0, and lysosome pH 4.0–5.0) [10]. Thus, it is a preferred strategy to construct a pH-triggered small molecule nano-prodrug to overcome multiple barriers for higher bioavailability and selective oral chemotherapy via dynamic physicochemical changes following stepwise responding to *in vivo* various pH microenvironment. Notably, particle sizes and surface properties are critical to overcoming physiological barriers [11]. The larger particle sizes can slow down the degradation of pH-triggered nano-prodrugs in the stomach, but can decrease the uptake by microfold (M) cells in Peyer's patches, which are a form of aggregated lymphatic tissue and the main sites for absorption of NPs in the small intestine [12]. In addition, the suitable particle sizes (~100 nm) facilitate blood circulation stability and tumor accumulation [13]. The surficial stronger hydrophobicity promotes small intestine absorption via easier biological mucosal adhesion and uptake of M cells [14], and electric neutrality is beneficial to uptake by M and tumor cells and stable blood circulation [15]. Hence, the pH-triggered nano-prodrugs with special physicochemical properties such as surficial strong hydrophobicity, electric neutrality and large-to-small size transition could overcome physiological barriers for improving drug bioavailability and tumor selectivity.

Chlorambucil (CLB) as an oral nitrogen mustard derivative and alkylating anti-cancer drug, has been widely applied for a variety of cancer diseases including chronic lymphocytic leukemia and solid tumors [16]. However, its disadvantages such as low water solubility, short half-life owing to rapid degradation in an aqueous environment, and serious side effects due to low specificity toward tumor cells limit its clinical applications [17–19]. Therefore, the use of CLB to construct pH-responsive small molecule nano-prodrug to improve its solubility, stability, bioavailability, and tumor selectivity is highly demanded for enhancing its oral chemotherapeutic effect comparted to other CLB-based oral nanomedicines. Notably, the carboxyl group in CLB is nonfunctional site when triggering interstrand and intrastrand linking of DNA [16]. Additionally, we have reported the pH-sensitive star-shaped ortho esters containing four

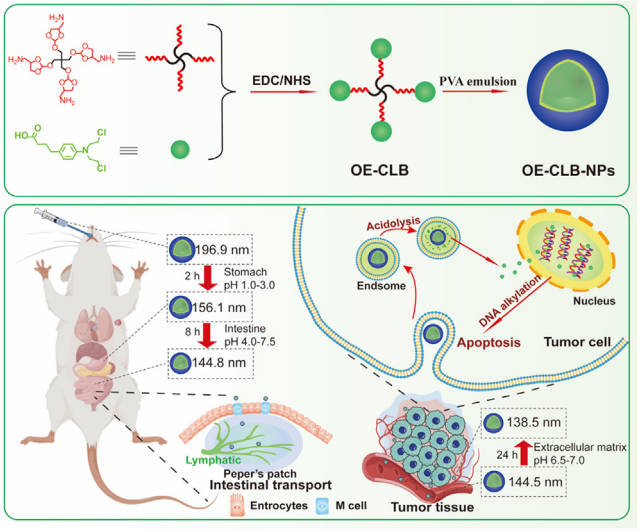

Scheme 1 – Schematic illustration of pH-triggered dynamic erosive small molecule nano-prodrugs for robust oral chemotherapy.

amino groups, whose degradation rate can be regulated by grafting hydrophobic or hydrophilic components [20]. Thus, the pH-triggered star-shaped hydrophobic CLB prodrug could be facilely synthesized via amide reaction between CLB and OE, and could further construct nano-prodrugs in the form of nanospheres by the O/W emulsion solvent evaporation method, therefore achieving long-term storage stability via multiple types of non-covalent interactions, enhanced gastrointestinal absorption and blood circulation stability via surficial strong hydrophobicity and electric neutrality as well as large-to-small size transition from stomach to small intestine following surficial progressive acid erosion, and improved tumoral accumulation and programmable targeted drug release via enhanced permeability and retention (EPR) effect and further acid erosion (Scheme 1).

2. Materials and methods

2.1. *Materials*

Triethylamine (TEA) and chloroform ($CHCl_3$) were dried with calcium hydride before use. Chlorambucil (CLB, 98%), N–hydroxy succinimide (NHS, 98%), 1-(3-dimethylaminopropyl)−3-ethylcarbodiimide hydrochloride (EDC, 98%), 3-(4,5-dimethylthiazol-2-yl)−2,5-diphenyltetrazolium bromide (MTT, 98%), silica gel for column chromatography (spherical, 200–300 mesh), 3-(2-benzothiazolyl)−7-(diethylamino)coumarin (coumarin 6.98%) and polyvinyl alcohol (PVA, 13,000–23,000 Da) were obtained from Macklin (Shanghai, China). (2,2′-((2,2-bis(((4-(aminomethyl)−1,3-dioxolan-2-yl)oxy)methyl)propane-1,3-diyl)bis(oxy))bis (1,3-diox-olane-4,2-diyl))dimethanamine (OE) was prepared as described before [20]. Human and murine hepatic cancer cell lines (HepG2 and H22), human breast cancer cell lines (MCF-7), human chronic myeloid leukemia cell lines (K562), and human pulmonary adenocarcinoma cell lines (A549) were obtained from Procell

Life Science&Technology Co., Ltd. (Wuhan, China). Male ICR mice (20–24 g) were acquired from Anhui Medical University (Hefei, China), and the care and use of animals followed the guidance of Anhui University Laboratory Animal Ethics and Management Committee (IACUC(AHU)−2023–012).

2.2. Synthesis and characterization of star-shaped CLB prodrug (OE-CLB)

CLB (400.0 mg, 1.315 mmol), EDC (378.0 mg, 1.972 mmol) and NHS (227.0 mg, 1.972 mmol) were dissolved in 10 ml of $CHCl_3$; the mixture was stirred for 4 h under nitrogen atmosphere. Then, OE (118.4 mg, 0.219 mmol) was added into above mixture and stirred for another 24 h at room temperature in dark. Afterwards, the crude product was dialyzed against ethanol (70%, v/v) via a dialysis bag (MWCO 500 Da), and purified through silica gel column chromatography using gradient elution of dichloromethane (CH_2Cl_2)/methanol (MeOH) from 50:1 to 10:1. Finally, OE-CLB was obtained with yield of 76.4% and its structure was determined using ^{1}H nuclear magnetic resonance spectroscopy (^{1}H NMR, Fourier 80, Bruker, Germany), and X-ray diffractometer (XRD, Smartlab 9 kW, RIGAKU, Japan).

2.3. Preparation and characterization of OE-CLB-based nano-prodrugs (OE-CLB-NPs) and coumarin-loaded OE-CLB-NPs (OE-CLB-NPs@ coumarin)

OE-CLB-NPs were prepared using the O/W emulsion solvent evaporation method [21]. In brief, OE-CLB (20.0 mg) was dissolved in 1 ml CH_2Cl_2; this mixture was added dropwise to 5 ml PVA aqueous solution (5%, w/v) and vortexed with a homogenizer for 1 min, and subsequently sonicated three times (10 s each time) at 50% amplitude using a handheld ultrasonic cell disruptor (UP-250, Ningbo Scientz Biotechnology Co.,Ltd., China). Afterwards, the emulsion was immediately poured into 20 ml PVA aqueous solution (0.3%, w/v) and stirred magnetically in an open beaker at room temperature for 3 h. Finally, OE-CLB-NPs were obtained after centrifugation at 9.0×10^3 rpm for 15 min and rinse using deionized water three times. OE-CLB-NPs@coumarin were prepared via the same method and the mass feeding ratio between OE-CLB-NPs and coumarin 6 was 10:1. The particle size transitions of OE-CLB-NPs were determined in various buffer solutions (pH 7.4, 7.0, 6.8, 6.0, 5.0 and 1.0), buffer solution with a continuous pH change from stomach pH to tumoral intracellular pH, foetal bovine serum (FBS), saline, simulated gastric juice and simulated intestinal juice at desired time points by a dynamic light scattering detector (DLS, Nano ZS90, Malvern Panalytical Ltd., UK) and/or transmission electron microscopy (TEM, JEM 2100, JEOL Ltd., Japan). Zeta potentials were measured in various buffer solutions (pH 7.4, 7.0, 6.8, 6.0, 5.0 and 1.0) by DLS.

2.4. Measurement of hydrolysis of ortho esters in OE-CLB-NPs

OE-CLB-NPs were dispersed in various buffer solutions (pH 7.4, 7.0, 6.8, 6.0, 5.0, and 1.0) at 37 °C and lyophilized at 0 h, 4 h, 12 h and 24 h. Then, the samples were measured via ^{1}H NMR, after being dissolved in deuterated chloroform ($CDCl_3$). The hydrolysis rate was confirmed by the ratio of integral areas between peaks at 8.05 and 8.11 ppm and peaks at 5.76, 8.05 and 8.11 ppm.

2.5. Measurement of in vitro CLB release from OE-CLB-NPs

1 ml OE-CLB-NPs containing 1.0 mg CLB were added into dialysis bags (MWCO 8–14 kDa), which were immersed into 5 ml of various buffer solutions (pH 7.4, 7.0, 6.8, 6.0, 5.0, and 1.0) containing 0.5 mol/l of sodium salicylate or that with a continuous pH change from stomach pH to tumoral intracellular pH. The dialysate was replaced at predetermined time points, and CLB contents in samples were determined using High Performance Liquid Chromatography (HPLC, UltiMate 3000, Thermo Fisher Scientific Inc., USA) with ODS C_{18} column (150 × 4.6 mm, 5 μm) and eluent of methanol/water/acetic acid (80/20/0.2, v/v) at UV–vis wavelength of 254 nm.

2.6. Determination of in vitro cytotoxicity

In brief, various tumor cells (MCF-7, HepG2, H22 and K562) were seeded into 96-well plates (5×10^3 /well) and cultured for 12 h. Then, OE-CLB-NPs and CLB with same gradient CLB concentration (1.875, 3.75, 7.5, 15, 30 and 60 μg/ml) were co-incubated with tumor cells for 48 h at 37 °C. Afterwards, the medium (RPMI-1640) was replaced by fresh one, and tumor cells were co-incubated with MTT aqueous solution (0.5 mg/ml) for another 4 h. Finally, the culture plates were determined at UV–vis absorption wavelength of 570 nm using a Microplate Reader (SpectraMax M2e, Molecular Devices, USA), after the medium was replaced by 150 μl dimethyl sulfoxide and shaken for 15 min.

2.7. Analysis of qualitative and quantitative cellular uptake

MCF-7, HepG2 and A549 were seeded on the coverslips in 6-well plates (5×10^3 /well) and cultured for 12 h. Then, OE-CLB-NPs@coumarin with the CLB concentration of 60 μg/ml were co-incubated with three types of tumor cells in 1 h and 4 h respectively for exploring time-dependent cellular uptake. The tumor cells were qualitatively observed and photographed using a laser scanning confocal microscope (CLSM, OLS4100, Olympus Corporation, Germany), after being sequentially washed twice by fresh phosphate buffer solution (PBS), immobilized for 10 min by 4% of paraformaldehyde, dyed for 2 min by Hoechst 33,258 and washed twice by fresh PBS.

OE-CLB-NPs and CLB with the drug concentration of 60 μg/ml were co-incubated with three types of tumor cells for 1 h and 4 h in 6-well plates, respectively. The cells were then washed twice, lysed for 30 min at 4 °C, suspended using a cell scraper, and centrifugated at 1.2×10^4 rpm for 10 min. Finally, the CLB content was confirmed using HPLC according to the above method in Section 2.5, after the supernatant was extracted with CH_2Cl_2 three times.

2.8. Analysis of apoptosis

Briefly, HepG2 and MCF-2 were inoculated into 6-well plates (5×10^3 per well) and cultured for 12 h, respectively. Then, OE-CLB-NPs and CLB with the drug concentration of 60 μg/ml were co-incubated with two types of tumor cells for 48 h. Afterwards, the tumor cells were collected via trypsin enzyme-digesting technique and centrifugation at 2.0×10^3 rpm for 5 min, and dyed using Annexin V-FITC and propidium iodide (PI) for 10 min. Finally, the apoptosis rate was analyzed via a flow cytometry (FCM, CytoFLEX, Beckman Coulter, USA).

2.9. Measurement of entering blood circulation

OE-CLB-NPs (20 mg/ml, 0.2 ml) were intragastrically administered to the ICR mice, and 0.5 ml of blood samples were taken from the orbit after 4 h. Then, the blood samples were centrifuged at 3×10^3 rpm for 10 min and the supernatant was observed and measured using TEM and TEM-energy dispersive spectrometer (EDS), after 50 μl of heparin sodium solution (1 mg/ml) was added into above blood samples.

2.10. Measurement of pharmacokinetics and in vivo biodistribution

In brief, the H22 tumor-bearing mice were established via injection of H22 cells (5×10^5/0.1 ml saline) into the left axilla of ICR mice. The mice were divided into 3 groups, with 18 mice in each group. When the tumor volumes reached about 150 mm^3, saline, and formulations (OE-CLB-NPs and CLB) with drug concentration (4.8 mg/kg) were intragastrically administered to the mice. When the mice were sacrificed in 1, 2, 4, 8, 12 and 24 h, the blood and various tissues (heart, liver, spleen, lung, kidney, and tumor) were surgically obtained and weighed. The drug content in each sample was measured via HPLC according to the above method in Section 2.5, after the sample was extracted for 24 h using 0.3 mol/l of hydrochloric acid-methanol solution and centrifugated at 9.0×10^3 rpm for 15 min. The oral relative bioavailability (RB) was confirmed via the following formula [22]:

$$\text{RB}\ (\%) = \frac{\text{AUC(OE} - \text{CLB} - \text{NPs)}}{\text{AUC(CLB)}} \times 100\%$$

Where *AUC(OE-CLB-NPs)* and *AUC(CLB)* refer to the area under the concentration-time curve of groups treated by OE-CLB-NPs and CLB, respectively.

2.11. Evaluation of in vivo tumor growth inhibition

The mice were divided into 3 groups, with 6 mice in each group. When the tumor volumes reached about 150 mm^3 in H22 tumor-bearing mice, saline, and formulations (OE-CLB-NPs and CLB) with drug concentration (0.25 mg/kg) were intragastrically administered to the mice daily, whose tumor size and body weight was measured every day. After seventeen days, main tissues (stomach, intestine, heart, liver, spleen, lung, kidney, and tumor) were surgically obtained, weighed, photographed, and sectioned for Hematoxylin-Eosin (H&E) and TUNEL staining. In addition, stomach and intestine were dissected to observe tissue integrity. The tumor inhibition ratio (IR) was confirmed via the following formula [23]:

$$\text{IR}\ (\%) = \frac{\text{Wc} - \text{Wt}}{\text{Wc}} \times 100\%$$

where Wt and Wc refer to the average tumor weight of groups treated by formulations (OE-CLB-NPs and CLB), and control group treated by saline, respectively.

2.12. Hemolysis assay

The fresh blood samples were surgically obtained from ICR mice and stabilized by anticoagulant sodium citrate (3.8%, w/v). Then, after the mixture was centrifuged at 5×10^3 rpm for 5 min and suspended with physiological saline, the red blood cells (RBCs) were co-cultured with OE-CLB-NPs in a series of concentrations (0.1 - 1.6 mg/ml) at 37 °C for 1 h. Double distilled water (ddH_2O) and physiological saline were used as positive and negative controls, respectively. Afterwards, the supernatant was collected by centrifugation at 9×10^3 rpm for 5 min and detected at the UV–vis absorption wavelength of 545 nm using a Microplate Reader.

2.13. Statistical analysis

Data were displayed as the mean ± SD and analyzed using SPSS. Comparisons were performed by one-way ANOVA ($^*P < 0.05$, $^{**}P < 0.01$ and $^{***}P < 0.001$).

3. Results and discussion

3.1. Preparation and characterization of OE-CLB and OE-CLB-NPs

As shown in Fig. 1A, to construct the pH-triggered dynamic erosive small molecule nano-prodrugs, the hydrophobic star-shaped CLB prodrug (OE-CLB) was first synthesized via the amide reaction between CLB and pH-sensitive star-shaped ortho esters containing four amino groups (OE) at the molar feeding ratio of 6:1. The excess CLB was removed via dialysis against 70% of ethanol/water and silica gel column chromatography. Its structure was confirmed via ^{1}H NMR. As displayed in Fig. 1B, the appearance of characteristic proton peak at 8.01 ppm (f', -CO–NH-, Fig. 1B(c)) and disappearance of that at 1.49 ppm (f', -NH_2, Fig. 1B(b)) suggested the formation of amide linkages. Moreover, the integral area ratio of 1:2 between characteristic proton peak at 5.82 ppm (b', -CH–O_3, Fig. 1B(c)) and that at 6.62 ppm (b, -CH=CH–CN-, Fig. 1B(c)) indicated the successful synthesis of OE-CLB. Additionally, as shown in Fig. 1C, OE-CLB exhibited crystalline structure with broad peak at 22.90° in comparison with many sharp peaks of CLB from 13° to 30° and broad peak of OE at 19.71° The result also suggested the successful synthesis of OE-CLB.

The small molecule nano-prodrugs as form of nanospheres were emulsified from the hydrophobic star-shaped CLB prodrug (OE-CLB) via the O/W emulsion solvent evaporation

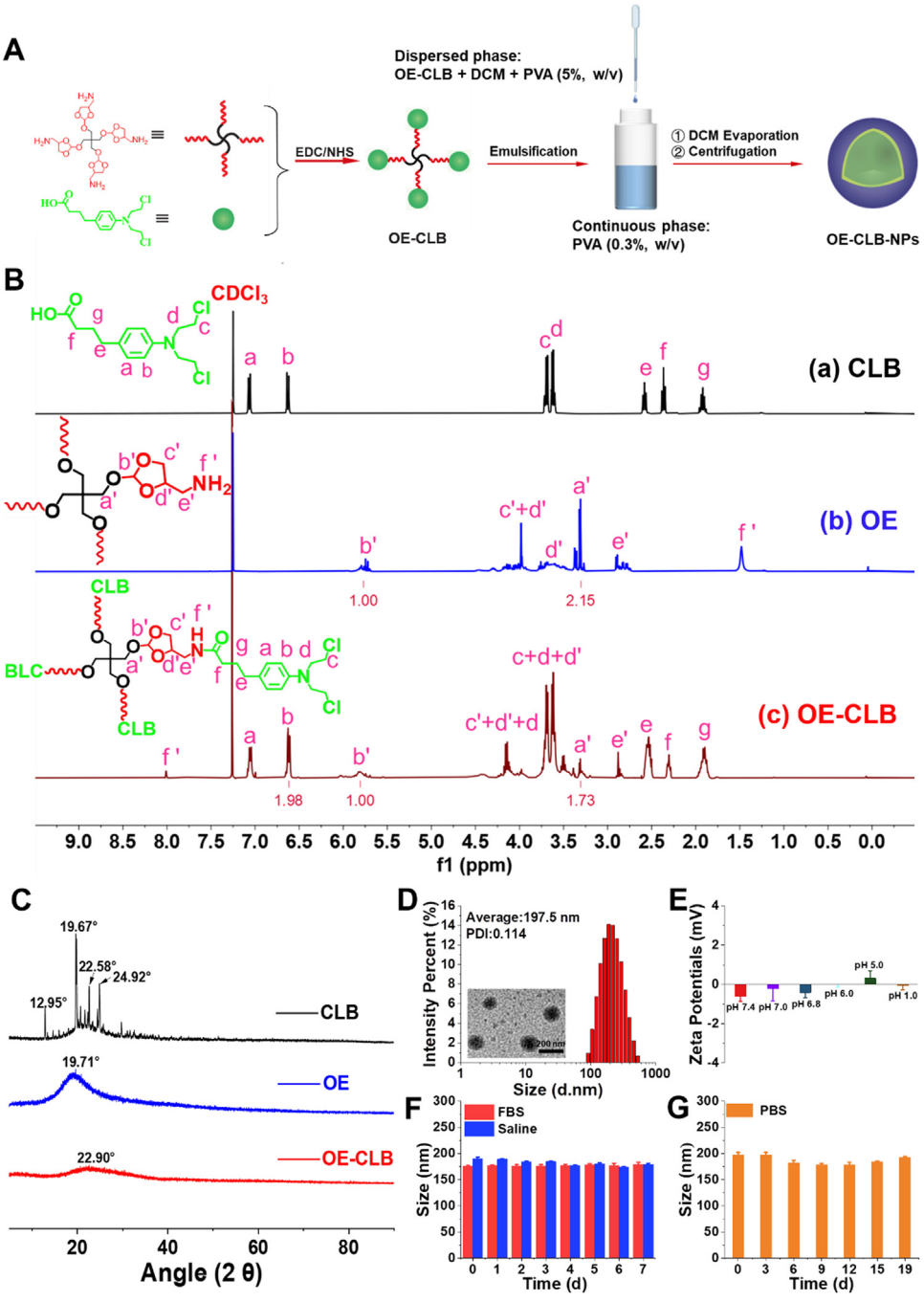

Fig. 1 – Schematic illustration of the synthesis of OE-CLB and preparation of OE-CLB-NPs (A), ^{1}H NMR (B) and XRD (C) of CLB, OE and OE-CLB, particle sizes at pH 7.4 (D), zeta potentials at various pHs (E), and change of particle sizes in FBS and saline for 7 d (F) and PBS (pH 7.4) for 19 d (G).

method (Fig. 1A) [21]. As seen in Table S1, the nano-prodrugs possessed extraordinarily high drug loading (68.16%) owing to the small proportion of excipients compared to other physically embedded or chemically linked CLB nanodrugs, by calculating the mass percentage of CLB in OE-CLB. As shown in Fig. 1D, the particle sizes were confirmed to be 197.5 nm by DLS. Their low polydispersity index (PDI) value (0.114) indicated uniform size distribution. In addition, their particle sizes about 160 nm observed by TEM were slightly smaller due to the shrinkage of NPs in a drying state during TEM sample preparation [24]. The larger initial size had a smaller specific surface area, which facilitated corrosion resistance in gastric juices [25]. As seen in Fig. 1E, zeta potentials such as −0.615 mV at pH 7.4, −0.198 mV at pH 7.0, −0.413 mV at pH 6.8, −0.008 mV at pH 6.0, 0.317 mV at pH 5.0 and −0.049 mV at pH 1.0 remained nearly electric neutrality, which was beneficial to gastrointestinal absorption, stability in blood vessel, and tumor accumulation [15]. Moreover, the particle sizes remain

the same in FBS and saline for 7 d and in PBS (pH 7.4) for 19 d (Fig. 1F and 1G), suggesting their long-term circulation and storage stability [26].

3.2. pH-triggered degradation of ortho ester linkages in OE-CLB-NPs

To investigate pH sensitivity to the microenvironment in gastrointestinal tract, blood vessel and tumor tissue, OE-CLB-NPs were suspended in various buffer solutions (pH 7.4, 7.0, 6.8, 6.0, 5.0 and 1.0) and lyophilized for ^{1}H NMR analysis at desired time points. As displayed in Fig. S1, the degradation of ortho ester linkages exhibited obvious pH and time dependence. On one hand, ortho ester linkages were fully hydrolyzed at gastric acid (pH 1.0) in 24 h, but less than 27.00% of these were hydrolyzed within the duration of gastric retention (1–4 h) [2]. The result suggested that stomach pH might not cause the disintegration of hydrophobic OE-CLB-NPs with larger initial size (~ 200 nm) in a short time, and might trigger the large-to-small size transition following the gradual erosion [25,27]. Additionally, about 40% and 60% of ortho ester linkages were degraded at duodenum and tumor intracellular pH (5.0) in 12 h and 24 h, respectively. The consequence suggested that duodenum pH might also lead to the tendency of particle sizes to decrease gradually following the degradation of ortho ester linkages during a short retention time (30–40 min) [2]. On the other hand, ortho ester linkages were not hydrolyzed at pH 7.4 and 7.0 in 24 h, indicating their stable chemical property during storage and circulation.

3.3. *Large-to-small size transition following degradation of ortho ester linkages*

To confirm the effect of degradation of ortho ester linkages on particle sizes, OE-CLB-NPs were suspended in various buffer solutions (pH 7.4, 7.0, 6.8, 6.0, 5.0 and 1.0) or that with a continuous pH change from stomach pH to tumoral intracellular pH, and their particle sizes were measured by DLS at desired time points. As shown in Fig. 2A-E, the change of particle sizes displayed obvious pH and time dependence. As displayed in Fig. 2B, the particle sizes remained the same at pH 7.4 and 7.0, and slightly minished from 196.9 nm to 175 nm at pH 6.8 and 6.0, but rapidly decreased from 197.5 nm to 120.2 nm at pH 5.0 and from 197.5 nm to 0 nm at pH 1.0 in 48 h owing to the progressive acid erosion following the degradation of ortho ester linkages. In addition, as shown in Fig. 2C and D, the average particle sizes also decreased at gastrointestinal analog fluid in 4 h. As seen in Fig. 2E, we further evaluated the change of particle sizes in continuously changing pH microenvironment. On one hand, the particle sizes decreased from 196.9 nm to 156.1 nm at pH 1.0 in stomach retention time (~ 2 h) [2], from 156.1 nm to 148.1 nm at pH 5.0 in duodenum retention time (~ 40 min) [2], from 148.1 nm to 145.7 nm at pH 6.0 in jejunum retention time (~ 1.5 h) [2], and then remain unchanged at pH 7.0 in ileum retention time (~ 6 h) [2]. The dynamic large-to-small size transition was beneficial to gastrointestinal absorption [28], thus improving oral bioavailability. On the other hand, the particle sizes (~ 144.8 nm) remained the same at pH 7.4 in 48 h, suggesting stable circulation and high tumor accumulation via size effect [29]. Moreover, the particle sizes continued to decrease from 144.5 nm to 138.5 nm at tumoral extracellular pH (6.8) in 24 h, further facilitating tumor penetration and cellular uptake upon arrival at target tumor sites via EPR effect [30,31]. The OE-CLB-NPs eventually disintegrated at tumoral intracellular pH (5.0) in 24 h. The intracellular efficient disintegration might promote the efficient release of CLB [32].

3.4. pH-triggered drug release

To explore the effect of large-to-small size transition on drug release, OE-CLB-NPs were dialyzed against buffer solutions (pH 7.4, 7.0, 6.8, 6.0, 5.0 and 1.0) or that with a continuous pH change from stomach pH to tumoral intracellular pH containing the cosolvent of sodium salicylate (0.5 mol/l), and the drug content in dialysate was measured using HPLC. As shown in Fig. 2F, the drug release from OE-CLB-NPs displayed distinct pH and time dependence. The amount of drug release was less than 10% at pH 7.4 and 7.0, and less than 20% at pH 6.8 and 6.0 in 48 h respectively, but accelerated in acidic buffer solutions (pH 5.0 and 1.0). In fact, as shown in Fig. 2G, on one hand, OE-CLB-NPs only remained in the stomach for 1–3 h, so that only a small amount of drug (about 10%) was released following large-to-small size transition via surficial progressive acid erosion. On the other hand, tumoral intracellular drug release was higher, after OE-CLB-NPs suffered from acidic erosion at gastrointestinal tract and tumor site, and disintegrated at tumoral intracellular pH. Notably, as seen in Fig. 2A, the drug released from OE-CLB-NPs was not CLB, but 3-amino-1,2-propanediol-bonded CLB via amide linkage, which could improve the solubility of CLB and might promote crosslinking with DNA [33–35].

3.5. *Improved tumoral cellular uptake, cytotoxicity, and apoptosis*

To investigate the influence of physicochemical properties of OE-CLB-NPs on pharmacological activity, cellular uptake, cytotoxicity, and apoptosis were performed using CLB as control (Fig. 3A). As shown in Fig. 3B and S2, OE-CLB-NPs@coumarin with particle sizes of 231.8 nm were easily internalized by HepG2, MCF-7 and A549 cells, and the uptake amount increased following time. Moreover, as seen in Fig. 3C-3E, the intracellular drug content in OE-CLB-NPs group was significantly higher than that in CLB group via quantitative analysis, owing to the suitable size (197.5 nm) and electric neutrality (−0.5 mV) of OE-CLB-NPs. In fact, OE-CLB-NPs were much easier to be internalized after suffering from *in vivo* large-to-small size transition. Notably, A549 cells have the same structure as the absorptive epithelial cells, so can be used as a tool to study the gastrointestinal absorption of NPs [36,37]. Thus, the result also suggested that OE-CLB-NPs could be effectively absorbed in intestine. As displayed in Fig. 3F-3I and S3, OE-CLB-NPs exhibited significantly stronger cytotoxicity than CLB on various tumor cells (MCF-7, HepG2, H22 and K562), owing to the improved cellular uptake, intracellular efficient drug release and easier crosslinking with DNA. Furthermore, apoptosis experiment was performed to prove whether cytotoxicity was caused by apoptosis. As

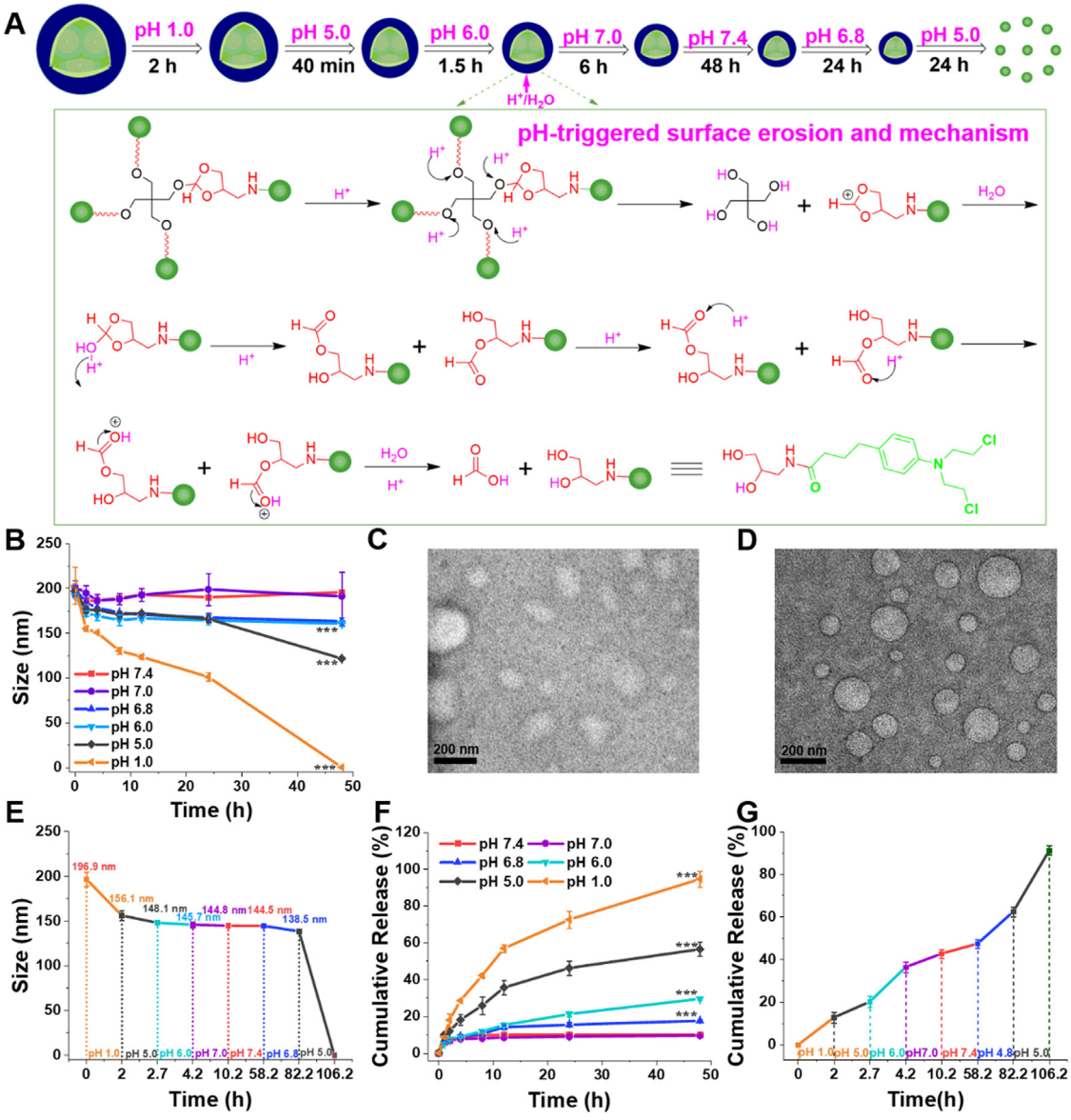

Fig. 2 – Schematic illustration of dynamic size change of OE-CLB-NPs from stomach pH to tumoral intracellular pH, and degradation mechanism of surface erosion (A), particle size change at various pHs (B), TEM images of OE-CLB-NPs in simulated gastric juice (C) and simulated intestinal juice (D) for 4 h, particle size transition at a continuous pH change from stomach pH to tumoral intracellular pH (E), and drug release at various pHs (F) and a continuous pH change from stomach pH to tumoral intracellular pH (G).

seen in Fig. 3J, the apoptosis rate of HepG2 was 43.0% and 52.3%, and that of MCF-7 was 36.1% and 60.2% induced by CLB and OE-CLB-NPs, respectively. The result was similar with that of cytotoxicity and suggested that apoptosis promoted cytotoxicity [38,39].

3.6. *Entering blood circulation through the gastrointestinal tract and hemolysis analysis*

To explore whether OE-CLB-NPs could enter blood circulation through gastrointestinal absorption, OE-CLB-NPs were intragastrically administered to the H22-bearing ICR mice, and blood sample was taken from the orbit after 4 h. The supernatant was determined using TEM and TEM-EDS after centrifugation. As shown in Fig. 3K, the smaller OE-CLB-NPs were found in blood sample compared to control treated by saline. Furthermore, OE-CLB-NPs containing C, N, O and Cl in the microregion were confirmed by TEM-EDS. These results suggested OE-CLB-NPs could successfully overcome gastrointestinal barrier and enter bloodstream, due to the favorable physicochemical properties such as large-to-small size transition, electric neutrality, and stronger hydrophobicity, which might promote small intestine absorption via M cells in Peyer's patches [11-15,27]. In addition, As seen in Fig. S4, less than 5% of hemolysis rate was induced by various concentrations of OE-CLB-NPs

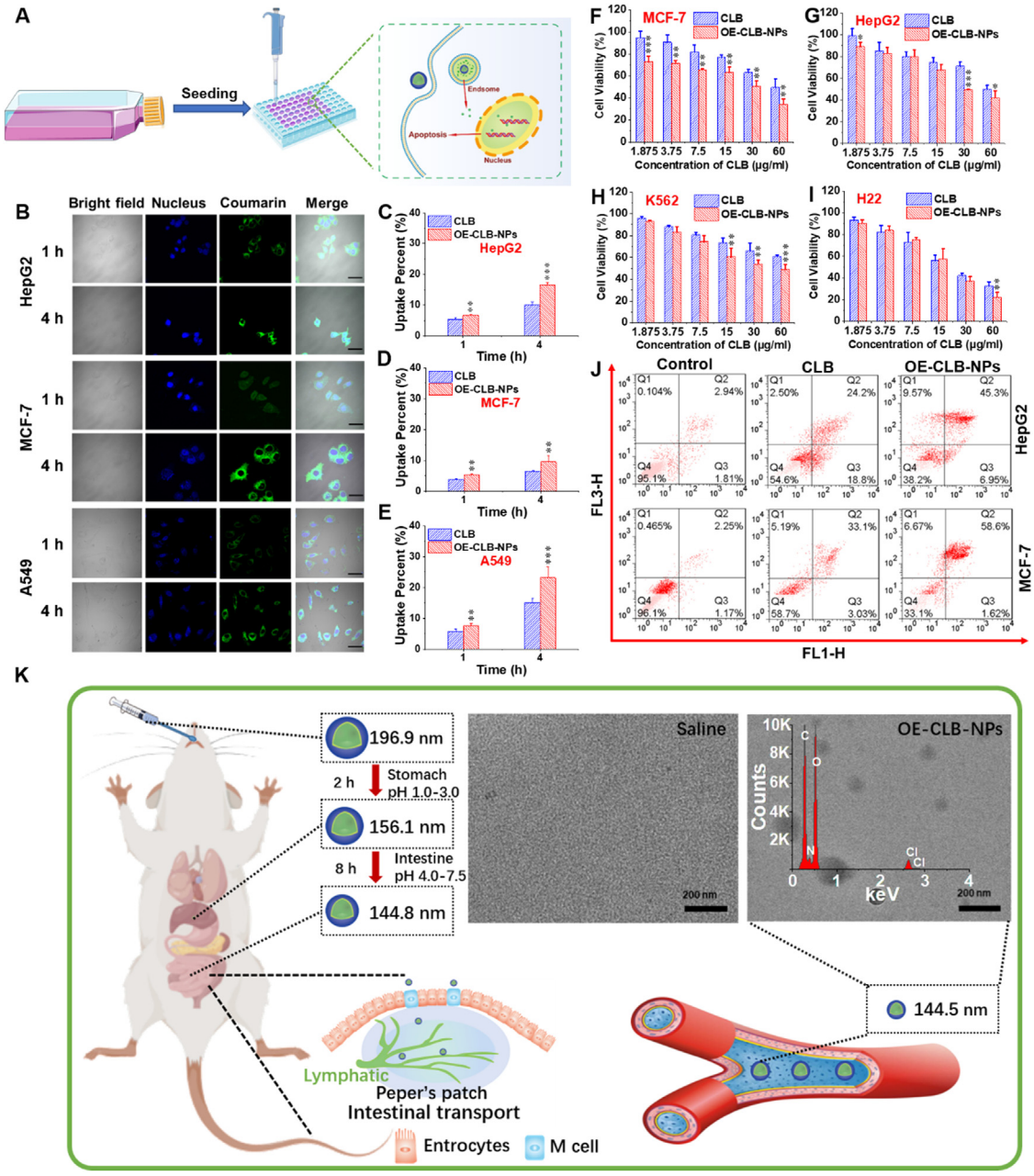

Fig. 3 – Schematic illustration of *in vitro* pharmacology experiment and mechanism (A), cellular uptake of OE-CLB-NPs measured by CLSM (B) and HPLC (C-E), *in vitro* cytotoxicity (F-I), and apoptosis (J); Schematic illustration of OE-CLB-NPs entering the bloodstream after suffering from gastrointestinal pH, and the blood samples observed and measured using TEM and TEM-EDS after centrifugation at 3 × 10^3 rpm for 10 min (K); Scale bar = 10 μm.

in comparison with the control, implying their fantastic hemocompatibility.

3.7. *Pharmacokinetics and in vivo biodistribution*

To evaluate the effect of physicochemical properties of OE-CLB-NPs on drug half-life, oral bioavailability, tumor accumulation and nonspecific distribution at normal tissues, pharmacokinetics and *in vivo* biodistribution were performed via oral administration and CLB content in various tissues was measured by HPLC at predetermined time points (Fig. 4A and S5). As shown in Fig. 4B and Table S2, OE-CLB-NPs exhibited higher plasma concentration than CLB at every time point, and their half-life was twice as long as that of CLB. Moreover, the area under the concentration-time curve (AUC) of OE-CLB-NPs was 3.6 times larger than that of CLB, implying the high oral relative bioavailability (358.72%). These results indicated that OE-CLB-NPs could be effectively absorbed orally into the bloodstream and were stable in the blood through electric neutrality, stronger hydrophobicity, and large-to-small size transition from gastrointestinal tract to blood vessels. As seen in Fig. 4C, OE-CLB-NPs displayed higher drug concentration

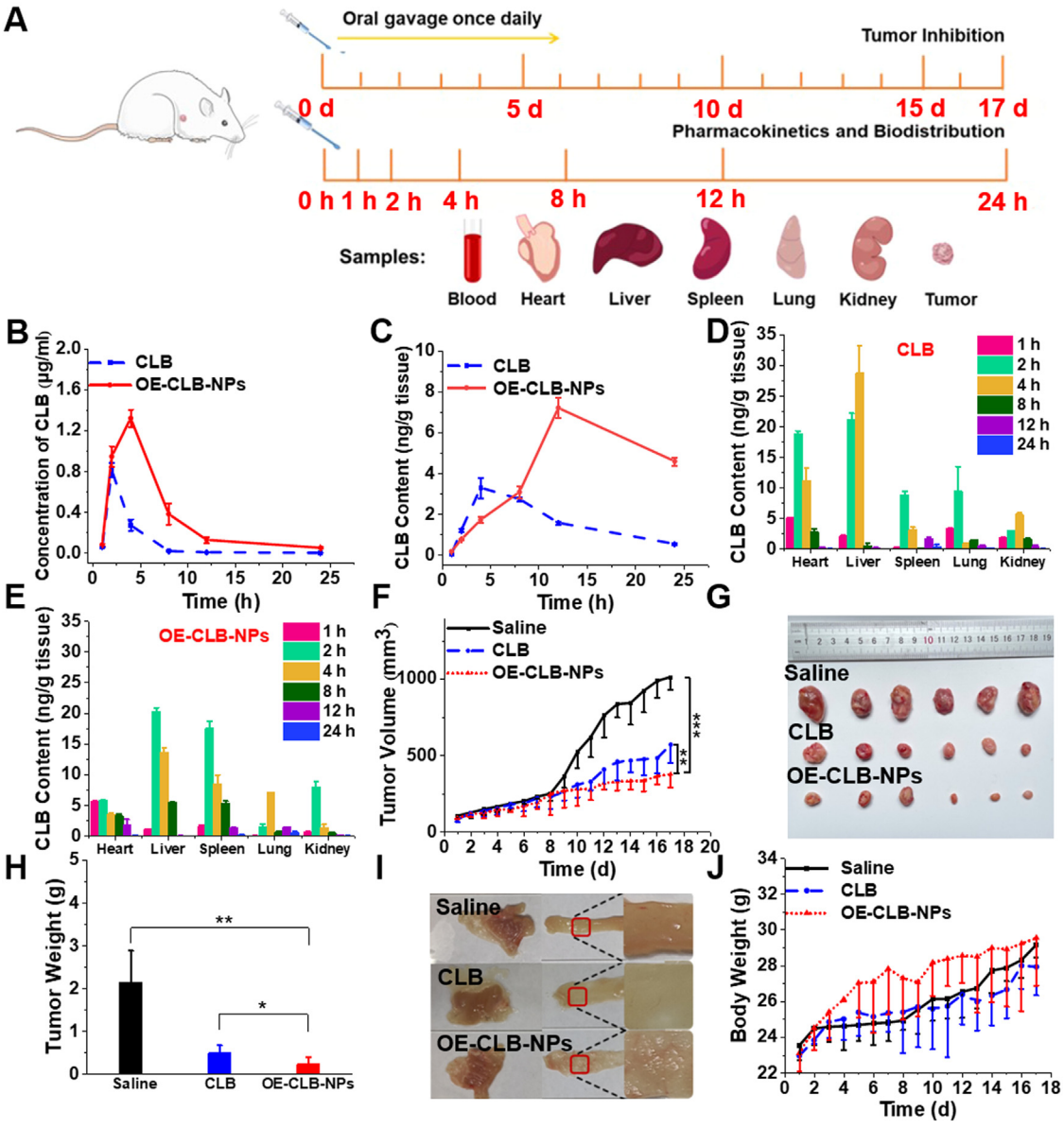

Fig. 4 – Schematic illustration of *in vivo* experiment about pharmacokinetics, drug biodistribution and tumor inhibition (A), change of CLB content in blood (B), tumor (C) and normal tissues (D and E) following the time course, change of tumor volume (F), image of tumor size (G), tumor weight (H), dissected gastrointestinal tract after treatment (I), and change of body weight (J).

than CLB at tumor tissues, indicating their improved tumor selectivity on account of tumoral extracellular further large-to-small size transition. In addition, as shown in Fig. 4D and 4E, OE-CLB-NPs exhibited lower drug concentration than CLB at normal tissues such as heart, liver, and lung, suggesting their lower side effects.

3.8. *Enhanced tumor growth inhibition*

To explore the influence of physicochemical properties of OE-CLB-NPs on tumor inhibition, various formulations (saline, CLB, and OE-CLB-NPs) were intragastrically administered to the H22-bearing ICR mice every day (Fig. 4A). After seventeen days, main tissues (stomach, intestine, heart, liver, spleen, lung, kidney, and tumor) were surgically obtained, weighed, photographed, and sectioned for H&E and TUNEL staining. As shown in Fig. 4F-4H, the tumor volume grew rapidly from 150 to 1000 mm^3 in saline group, but grew slowly in CLB formulations. OE-CLB-NPs exhibited the stronger antitumor activity than CLB, according to the slower tumor growth, smaller tumor size and weight, higher IR (88.69%), and more severe tumor damage (Fig. 5). It could attribute to their improved gastrointestinal absorption, tumor accumulation, cellular uptake, and cytotoxicity following the dynamic large-to-small size transition from gastrointestinal tract to tumor site. Additionally, as displayed in Fig. 4I, 4J and 5, the CLB caused a decrease in the number of blood vessels and injury at the gastrointestinal tract, and further made the body weight

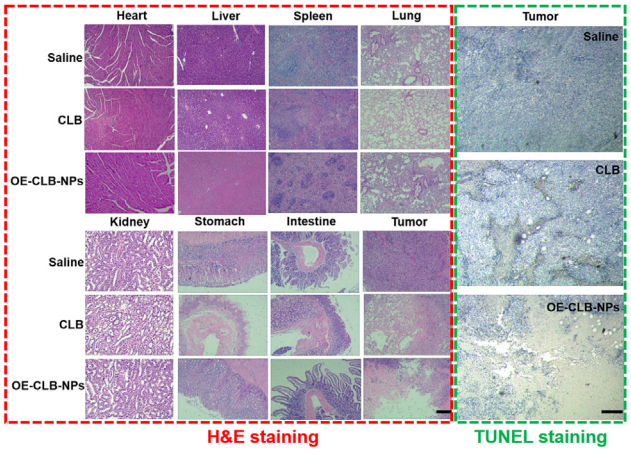

Fig. 5 – Histological analysis by H&E staining and TUNEL staining; Scale bar = 100 μm.

decrease obviously from Day 12 to Day 16, suggesting its serious side effects. Inversely, the gastrointestinal vascularity and integrity were normal and body weight gone up steadily in OE-CLB-NPs group through seventeen days compared to that treated by saline, although a small amount of drug was released following *in vivo* dynamic size change. The results indicated that pH-triggered dynamic erosive small molecule nano-prodrugs could significantly enhance oral chemotherapy while decreasing side effects.

4. Conclusion

This work successfully developed the pH-triggered dynamic erosive small molecule nano-prodrugs based on *in vivo* significant pH changes among gastrointestinal tract, blood vessels and tumor tissues. Their favorable physicochemical properties such as extraordinary high drug loading (68.16%), electric neutrality, strong hydrophobicity, and dynamic large-to-small size transition ranging from gastrointestinal pH to tumoral pH, could be beneficial to circumventing oral physiologic barriers in gastrointestinal tract, blood vessels and tumor tissues in comparison with other oral nanomedicines, and further promote gastrointestinal absorption, circulation stability, tumor accumulation, cellular uptake, and cytotoxicity, therefore achieving significant tumor growth inhibition while decreasing side effects on normal tissues. Thus, the pH-triggered dynamic erosive small molecule nano-prodrugs exhibit the superior characteristics such as simple synthesis, defined structure, high drug loading efficiency, and highly selective oral chemotherapy appealing for clinical transformation, although comprehensive preclinical and clinical evaluation still need to be further explored.

Conflicts of interest

The authors report no conflicts of interest. The authors alone are responsible for the content and writing of this article.

Acknowledgements

This work was supported by the Anhui Engineering Technology Research Center of Biochemical Pharmaceutical (Bengbu Medical College), the National Natural Science Foundation of China (No. 51803001), the Research Foundation of Education Department of Anhui Province of China (No. KJ2018ZD003, KJ2018A0006 and KJ2019A0015), and the Academic and Technology Introduction Project of Anhui University (AU02303203).

Appendix A. Supplementary data

Supplementary material associated with this article can be found, in the online version, at doi:10.1016/j.ajps.2023.100832.

References

[1] El Moukhtari SH, Rodriguez-Nogales C, Blanco-Prieto MJ. Oral lipid nanomedicines: current status and future perspectives in cancer treatment. Adv Drug Deliv Rev 2021;173:238–51.
[2] Alqahtani MS, Kazi M, Alsenaidy MA, Ahmad MZ. Advances in oral drug delivery. Front Pharmacol 2021;12:1–21.
[3] Ahadian S, Finbloom JA, Mofidfar M, Diltemiz SE, Nasrollahi F, Davoodi E, et al. Micro and nanoscale technologies in oral drug delivery. Adv Drug Deliv Rev 2020;157:37–62.
[4] Parodi A, Buzaeva P, Nigovora D, Baldin A, Kostyushev D, Chulanov V, et al. Nanomedicine for increasing the oral bioavailability of cancer treatments. J Nanobiotechnology 2021;19:1–19.
[5] Lee Y, Kamada N, Moon JJ. Oral nanomedicine for modulating immunity, intestinal barrier functions, and gut microbiome. Adv Drug Deliv Rev 2021;179:114021.
[6] Rajput A, Pingale P, Telange D, Chalikwar S, Borse V. Lymphatic transport system to circumvent hepatic metabolism for oral delivery of lipid-based nanocarriers. J Drug Deliv Sci Technol 2021;66:102934.
[7] Cote B, Rao D, Alani AWG. Nanomedicine for drug delivery throughout the alimentary canal. Mol Pharm 2022;19:2690–711.
[8] Etter EL, Mei KC, Nguyen J. Delivering more for less: nanosized, minimal-carrier and pharmacoactive drug delivery systems. Adv Drug Deliv Rev 2021;179:113994.
[9] Liu G, Lovell JF, Zhang L, Zhang Y. Stimulus-responsive nanomedicines for disease diagnosis and treatment. Int J Mol Sci 2020;21:1–44.
[10] Bazban-Shotorbani S, Hasani-Sadrabadi MM, Karkhaneh A, Serpooshan V, Jacob KI, Moshaverinia A, Mahmoudi M. Revisiting structure-property relationship of pH-responsive polymers for drug delivery applications. J Control Release 2017;253:46–63.
[11] Zhang T, Zhu G, Lu B, Qian Z, Peng Q. Protein corona formed in the gastrointestinal tract and its impacts on oral delivery of nanoparticles. Med Res Rev 2021;41:1835–50.
[12] Pandya P, Giram P, Bhole RP, Chang HI, Raut SY. Nanocarriers based oral lymphatic drug targeting: strategic bioavailability enhancement approaches. J Drug Deliv Sci Technol 2021;64:102585.
[13] Bai S, Zhang Y, Li D, Shi X, Lin G, Liu G. Gain an advantage from both sides: smart size-shrinkable drug delivery nanosystems for high accumulation and deep penetration. Nano Today 2021;36:101038.

[14] Wang W, Yan X, Li Q, Chen Z, Wang Z, Hu H. Adapted nano-carriers for gastrointestinal defense components: surface strategies and challenges. Nanomed-Nanotechnol 2020;29:102277.
[15] Zhang A, Meng K, Liu Y, Pan Y, Qu W, Chen D, Xie S. Absorption, distribution, metabolism, and excretion of nanocarriers *in vivo* and their influences. Adv Colloid Interfac 2020;284:102261.
[16] Maeda R, Bando T, Sugiyama H. Application of DNA-alkylating pyrrole-imidazole polyamides for cancer treatment. ChemBioChem 2021;22:1538–45.
[17] Wang X, Cao Y, Yan H. Chlorambucil loaded in mesoporous polymeric microspheres as oral sustained release formulations with enhanced hydrolytic stability. Mater Sci Eng C 2018;91:564–9.
[18] Nowak-Jary J, Machnicka B, Kozioł JJ. Cytotoxicity of chlorambucil immobilized on magnetic iron oxide nanoparticles Fe_3O_4. Micro Nano Lett 2021;16:515–23.
[19] Hu X, Liu R, Zhang D, Zhang J, Li Z, Luan Y. Rational design of an amphiphilic chlorambucil prodrug realizing self-assembled micelles for efficient anticancer therapy. ACS Biomater Sci Eng 2018;4:973–80.
[20] Xu Y, Wang S, Yang L, Dong Y, Zhang Y, Yan G, et al. pH-sensitive micelles self-assembled from star-shaped TPGS copolymers with ortho ester linkages for enhanced MDR reversal and chemotherapy. Asian J Pharm Sci 2021;16:363–73.
[21] Beig A, Feng L, Walker J, Ackermann R, Hong JKY, Li T, et al. Development and characterization of composition-equivalent formulations to the sandostatin LAR® by the solvent evaporation method. Drug Deliv Transl Res 2022;12:695–707.
[22] Xiong S, Liu W, Zhou Y, Mo Y, Liu Y, Chen X, et al. Enhancement of oral bioavailability and anti-parkinsonian efficacy of resveratrol through a nanocrystal formulation. Asian J Pharm Sci 2020;15:518–28.
[23] Zhang H, Zhang J, Li Q, Song A, Tian H, Wang J, et al. Site-specific MOF-based immunotherapeutic nanoplatforms via synergistic tumor cells-targeted treatment and dendritic cells-targeted immunomodulation. Biomaterials 2020;245:119983.
[24] Huang P, Wang D, Su Y, Huang W, Zhou Y, Cui D, et al. Combination of small molecule prodrug and nanodrug delivery: amphiphilic drug–drug conjugate for cancer therapy. J Am Chem Soc 2014;136:11748–56.
[25] Guo H, Zheng X, Luo X, Mai B. Leaching of brominated flame retardants (BFRs) from BFRs-incorporated plastics in digestive fluids and the influence of bird diets. J Hazard Mater 2020;393:122397.
[26] Wang X, Deng B, Yu M, Zeng T, Chen Y, Hu J, et al. Constructing a passive targeting and long retention therapeutic nanoplatform based on water-soluble, non-toxic and highly-stable core–shell poly(amino acid) nanocomplexes. Biomater Sci 2021;9:7065.
[27] Hu J, Yuan X, Wang F, Gao H, Liu X, Zhang W. The progress and perspective of strategies to improve tumor penetration of nanomedicines. Chinese Chem Lett 2020;32:1341–7.
[28] Rewatkar P, Kumeria T, Popat A. Size, shape and surface charge considerations of orally delivered nanomedicines. Nanotechnol Oral Drug Deliv 2020:143–76.
[29] Dutta D, Ke W, Xi L, Yin W, Zhou M, Ge Z. Block copolymer prodrugs: synthesis, self-assembly, and applications for cancer therapy. WIREs Nanomed Nanobiotechnol 2020;12:1–19.
[30] Wu J. The enhanced permeability and retention (EPR) effect: the significance of the concept and methods to enhance its application. J Pers Med 2021;11:771.
[31] Fang J, Islam W, Maeda H. Exploiting the dynamics of the EPR effect and strategies to improve the therapeutic effects of nanomedicines by using EPR effect enhancers. Adv Drug Deliv Rev 2020;157:142–60.
[32] Mei H, Cai S, Huang D, Gao H, Cao J, He B. Carrier-free nanodrugs with efficient drug delivery and release for cancer therapy: from intrinsic physicochemical properties to external modification. Bioact Mater 2022;8:220–40.
[33] Gómez-Canela C, Campos B, Barata C, Lacorte S. Degradation and toxicity of mitoxantrone and chlorambucil in water. Int J Environ Sci Technol 2015;12:633–40.
[34] Chen W, Han Y, Peng X. Aromatic nitrogen mustard-based prodrugs: activity, selectivity, and the mechanism of DNA cross-linking. Chem Eur J 2014;20:7410–18.
[35] Singh RK, Kumar S, Prasad DN, Bhardwaj TR. Therapeutic journery of nitrogen mustard as alkylating anticancer agents: historic to future perspectives. Eur J Med Chem 2018;151:401–33.
[36] Cortez-Jugo C, Czuba-Wojnilowicz E, Tan A, Caruso F. A focus on "bio" in bio–nanoscience: the impact of biological factors on nanomaterial interactions. Adv Healthc Mater 2021;10:1–21.
[37] Forbes B. Human airway epithelial cell lines for *in vitro* drug transport and metabolism studies. Pharm Sci Technol Today 2000;3:18–27.
[38] Wang Z, Wang D, Liu X, Wu H, Liu Y, Ge Y, et al. Dynamic carboxymethyl chitosan-based nano-prodrugs precisely mediate robust synergistic chemotherapy. Carbohydr Polym 2022;291:119671.
[39] Atmaca H, İlhan S, Batır MB, Pulat CC, Güner A, Bektaş H. Novel benzimidazole derivatives: synthesis, *in vitro* cytotoxicity, apoptosis and cell cycle studies. Chem Biol Interact 2020;327:109163.